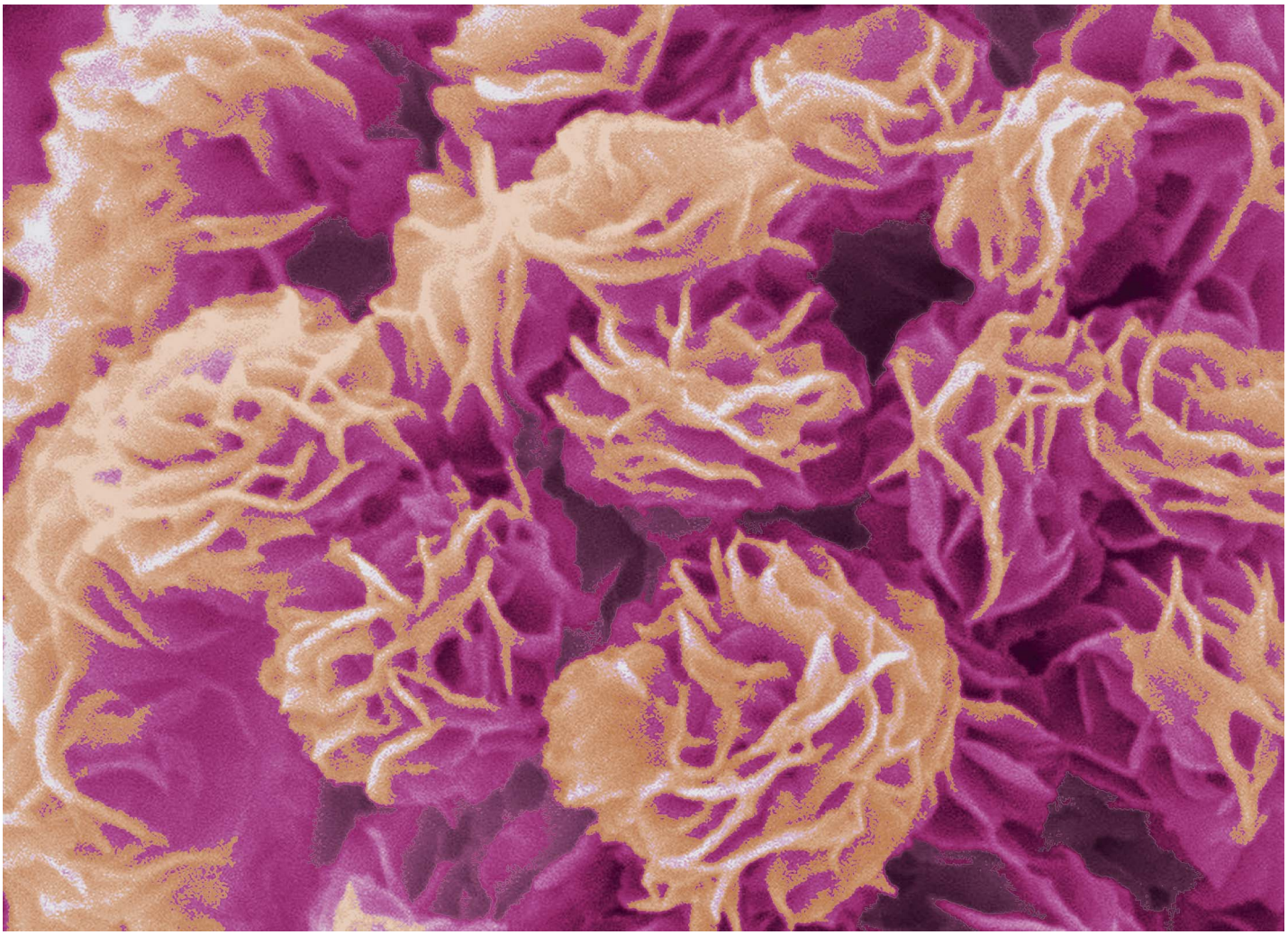

Showcasing research from Professor Jinyun Liu's laboratory, College of Chemistry and Materials Science, Anhui Normal University, Anhui, P.R. China.

A novel rose-with-thorn ternary MoS_2@carbon@polyaniline nanocomposite as a rechargeable magnesium battery cathode displaying stable capacity and low-temperature performance

A novel rose-with-thorn ternary MoS_2@carbon@polyaniline nanocomposite composed of carbon and polyaniline nanoneedles co-coated on MoS_2 is developed. The composite-based Mg battery displays a good capacity, and a recoverable rate-performance after repeated measurements. In addition, a stable capacity when cycling under a low temperature of −5 °C is also achieved, indicating a good potential for applications.

As featured in:

See Jinyun Liu, Tianli Han, Jinjin Li *et al.*, *Nanoscale Adv.*, 2021, **3**, 5576.

ROYAL SOCIETY OF CHEMISTRY

rsc.li/nanoscale-advances

Registered charity number: 207890

Nanoscale Advances

ROYAL SOCIETY OF CHEMISTRY

PAPER

View Article Online
View Journal | View Issue

Cite this: *Nanoscale Adv.*, 2021, **3**, 5576

A novel rose-with-thorn ternary MoS_2@carbon@polyaniline nanocomposite as a rechargeable magnesium battery cathode displaying stable capacity and low-temperature performance†

Jinyun Liu, ‡*[a] Yan Zhong,‡[a] Xuelian Li,[a] Tongxin Ying,[a] Tianli Han*[a] and Jinjin Li *[b]

Developing high-performance cathode materials for magnesium (Mg) batteries is of great significance. Here, a novel rose-with-thorn ternary MoS_2@C@polyaniline (PANI) nanocomposite composed of carbon and PANI nanoneedles co-coated on rose-like MoS_2 is developed. The conductive PANI needles on the surface of MoS_2 improve the conductivity, and the inner MoS_2 is wrapped by a carbon layer which is beneficial for the aniline coating. The MoS_2@C@PANI-based Mg battery cathode displays a good capacity of 114 mA h g^{-1} after 100 cycles, and a recoverable rate-performance after repeated measurements. In addition, a stable capacity of 105 mA h g^{-1} when cycled at a low temperature of −5 °C is also achieved, indicating good potential for applications.

Received 16th June 2021
Accepted 20th August 2021

DOI: 10.1039/d1na00445j

rsc.li/nanoscale-advances

Introduction

Recently, magnesium (Mg) batteries have attracted much attention due to their outstanding advantages including no dendrite growth and stable performance.[1–3] However, current Mg batteries still have some shortcomings, including slow ion transport, easy collapse of the structure, difficulty in deintercalation and insertion of Mg ions and the insufficient performance of Mg batteries in some special application conditions, such as different temperatures.[4,5] In order to address these problems, a large number of studies have been conducted.[6,7] In view of the low crystallinity of the cathode materials, even small changes in the preparation process will cause huge differences in the performance. Studies have been conducted to accelerate the extraction of Mg ions to promote the performance of batteries. For example, Zuo *et al.* used a spinel $Mg(Mg_{0.5}V_{1.5})O_4$ cathode to accelerate the Mg^{2+} ion extraction kinetics.[8] The capacity was 102 mA h g^{-1} over 100 cycles. Du *et al.* used a simple template-directed selenization reaction to construct thin-film-assembled hollow CuSe nanocubes at room temperature.[9] Copper selenide $Cu_{2-x}Se$ was synthesized by a solution method, and the copper ions in the sublattice based on Se-could be reversibly replaced by Mg^{2+} ions.[10] Because of the same face-centered cubic Se^{2-} sublattice, $Cu_{2-x}Se$ and MgSe unit cell sizes are similar and the energy barrier is low, which improves the cycling stability. Based on the above research, it is found that multiple nanocomposites would improve the performance of the cathode, thereby improving the cycle capacity and stability.

In recent years, biomimetic technology has been introduced into the research of rechargeable batteries, which improves the capacity and cycle life. For example, Shen *et al.* developed a composite material with a cucumber-like structure,[11] which was characterized by flexibility and self-support. It buffered the volumetric change and improved the conductivity. Tao *et al.* used kapok fibers to synthesize fish-scale carbon nanosheets for lithium-sulfur batteries,[12] which have an excellent capacity retention rate of up to 95.4% after 90 cycles at 0.4 A g^{-1}. Zuo *et al.* synthesized a flower-like structure of V_2O_5@polyaniline (PANI), by insertion of aniline into the V_2O_5 interlayer,[13] resulting in the composite having a larger gap between layers, thereby improving the battery performance. Inspired by the ultra-strong capillarity of wood's aligned hierarchical microchannels, Miao *et al.* developed a nanofibrous organic cathode for sodium ion batteries, which displayed rapid ionic/electronic transport properties and ultrafast reaction kinetics.[14] In addition, an agaric-like anode of porous carbon decorated with

[a]*Key Laboratory of Functional Molecular Solids, Ministry of Education, Anhui Provincial Engineering Laboratory for New-Energy Vehicle Battery Energy-Storage Materials, College of Chemistry and Materials Science, Anhui Normal University, Wuhu, Anhui 241002, P. R. China. E-mail: jyliu@ahnu.edu.cn; hantianli@ahnu.edu.cn*

[b]*National Key Laboratory of Science and Technology on Micro/Nano Fabrication, Department of Micro/Nano-electronics, Shanghai Jiao Tong University, Shanghai 200240, P. R. China. E-mail: lijinjin@sjtu.edu.cn*

† Electronic supplementary information (ESI) available: Supplementary figures and table. See DOI: 10.1039/d1na00445j

‡ These authors contributed equally to this work.

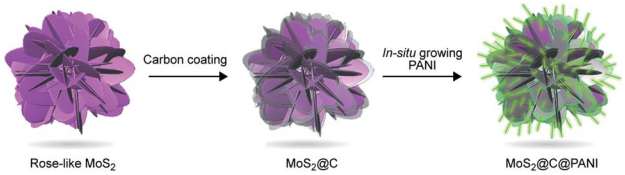

Fig. 1 Illustration of the preparation of ternary MoS_2@C@PANI.

MoO_2 nanoparticles was reported, which had a good rate capability, high capacity and long cycling lifespan for lithium and sodium storage.[15] From these findings, we can see that the biomimetic structure has great potential for developing high-performance Mg batteries. However, the design and performance enhancement mechanism of biomimetic structures still remain as challenges.

Here, inspired by the special structure of rose, we developed a novel ternary nanocomposite with a rose-with-thorn structure. The carbon-coated rose-like molybdenum disulfide (MoS_2) is then coated with thorn-shaped PANI, forming a MoS_2@C@PANI nanocomposite, as illustrated in Fig. 1. The preparation process is presented in the ESI.† The conductive PANI nanoneedles *in situ* grown on the surface can improve the conductivity; the inner MoS_2 is wrapped by a carbon layer, which is beneficial for the polymer coating. The results show that the cathode has a high Mg-storage performance and a good stability at low temperatures.

Results and discussion

Fig. 2a and b show the scanning electron microscopy (SEM) images of flower-shaped MoS_2 with a size of about 400–500 nm. The transmission electron microscopy (TEM) image in Fig. 2cshows the flower structure, and the petals are layered. The coated carbon layer makes the surface of MoS_2 rough, as shown in Fig. 2d and e. The TEM image in Fig. 2fshows the coating of the carbon layer. The carbon layer enables nanoneedle-like PANI to be efficiently coated. The SEM image of MoS_2@C@PANI is shown in Fig. 2g and h and the TEM image is shown in Fig. 2i. High-resolution TEM (HRTEM) images are displayed in Fig. 2j and k. The thickness of the PANI layer is about 40–50 nm; however the crystalline lattice of the inner MoS_2 is not clear because of the PANI coating. The SEM and elemental mapping images displayed in Fig. 3 verify the uniform distribution of Mo, S, N and C.

Fig. 4a shows the X-ray diffraction (XRD) patterns. The diffraction peaks are assigned to MoS_2 (JCPDS card no. #75-1539). The disappearance of the peak at about 15° was caused by the carbon coating, and the broad peak at 17.5° is ascribed to carbon. In addition, the peak at about 58° is not clear for the composite; instead, a new peak appears, which is indexed to the crystal plane (008) of MoS_2. The energy dispersive X-ray spectroscopy (EDS) spectrum (Fig. 4b) confirms the elements, which are consistent with the mapping images.[16] Thermogravimetric analysis (TGA) curves are shown in Fig. 4c. The weight loss of the MoS_2@C@PANI composite between 300 and 380 °C is attributed to the weight loss after oxidation of MoS_2. The loss from 380 to 450 °C is ascribed to C and PANI, which is about 33% calculated from 55 − 22%. So, from the TGA curve of the composite, the percentage of MoS_2 is calculated to be 1 − 33 − 10% (moisture) ≈57%.

Fig. 5a shows the Fourier transform infrared spectroscopy (FTIR) spectra. The peak at 1569 cm^{-1} is from C–C.[17] The 1116 and 799 cm^{-1} peaks are indexed to C–H bending.[18] The Raman spectra in Fig. 5bshow prominent Raman-active peaks. The peaks of sulfide are observed at 403 and 376 cm^{-1}. The peaks at

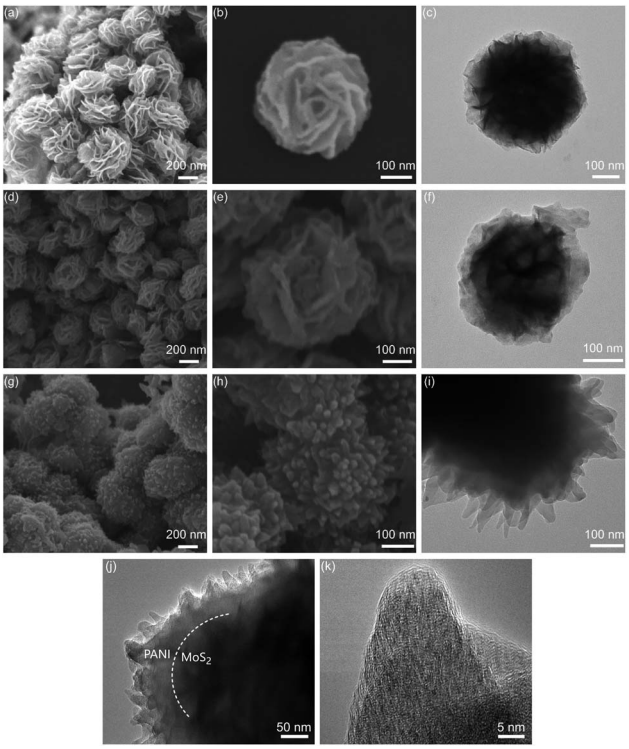

Fig. 2 SEM images of (a and b) flower-shaped MoS_2, (d and e) MoS_2@C, and (g and h) MoS_2@C@PANI. TEM images of the (c) bare MoS_2, (f) MoS_2@C composite and (i) MoS_2@C@PANI. (j and k) HRTEM images of MoS_2@C@PANI. The dashed line in j indicates the boundary between MoS_2 and PANI.

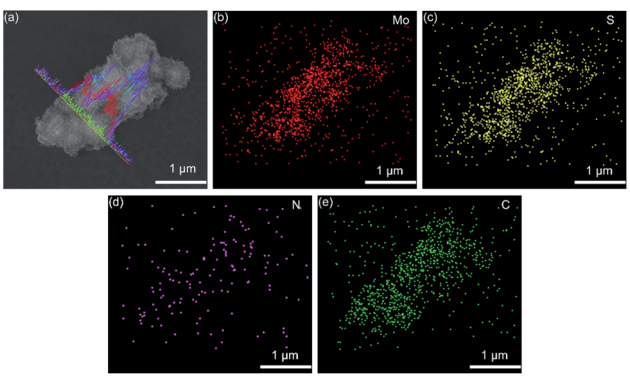

Fig. 3 (a) SEM and (b–e) elemental mapping images of MoS_2@C@PANI. Line-scan profiles are inserted in (a).

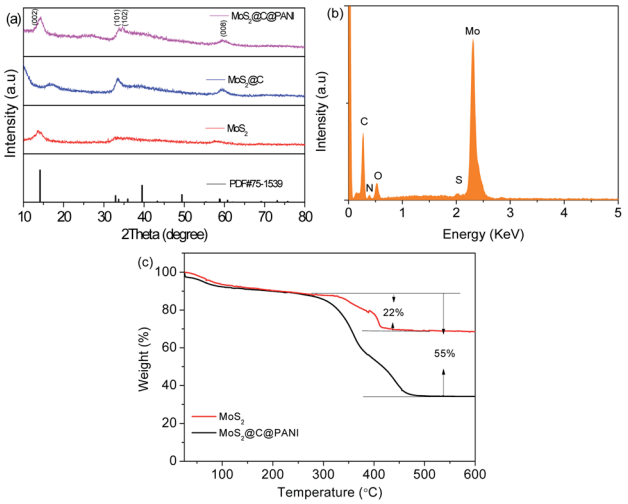

Fig. 4 (a) XRD patterns of MoS_2, MoS_2@C, and MoS_2@C@PANI. (b) EDS spectrum of MoS_2@C@PANI. (c) TGA curve of bare MoS_2 and MoS_2@C@PANI.

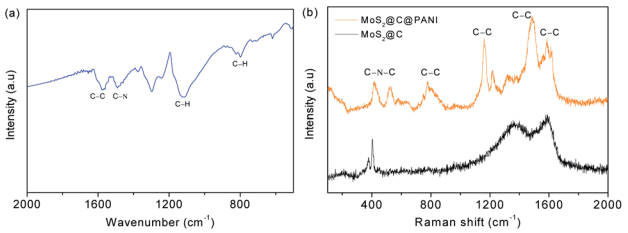

Fig. 5 (a) FTIR spectrum of MoS_2@C@PANI. (b) Raman spectra of bare MoS_2 and the MoS_2@C@PANI composite.

1365 and 1587 cm^{-1} are assigned to the D-band and G-band of carbon, respectively. In MoS_2@C@PANI, the peaks at 1587, 1485, 1324, 1162 and 780 cm^{-1} are from C–C.[19] The peaks at 1384 and 1162 cm^{-1} are ascribed to C–N and C–H, respectively, which verify PANI.[20] Fig. 6 shows the X-ray photoelectron spectroscopy (XPS) spectra. The survey spectrum in Fig. 6a verifies the composition. The Mo 3d spectrum is shown in Fig. 6b. There are two peaks at 228.8 and 231.7 eV which are attributed to Mo $3d_{3/2}$ and Mo $3d_{5/2}$, respectively.[21] A minor peak at 225.5 eV shows the presence of S 2s.[22] In Fig. 6c, the peaks are indexed to S $2p_{3/2}$ and S $2p_{1/2}$.[23] In Fig. 6d, the N 1s spectrum is deconvoluted into three peaks at 397.5, 398.5, and 400.5 eV.[24] The peaks at 284.0, 285.1, and 288.0 eV are assigned to C–C, C–OH, and C=O,[25] respectively, as shown in Fig. 6e.

Fig. 7a shows the charge–discharge curves of MoS_2@C@PANI cycled at 100 mA g^{-1}. As shown in Fig. 7b, when cycled at 100 mA g^{-1}, the capacity is 114 mA h g^{-1} after 100 cycles. Moreover, the coulombic efficiency exceeds 99%. Compared to pure MoS_2, it shows a better cycling performance. It is noted that the PANI coating in the composite system also contributes to the capacity,[26] which improves the overall performance. When compared to some other cathodes, the developed MoS_2@C@PANI is also competitive, as shown in Table S1 (ESI†). Fig. 7c shows the CV profile of the MoS_2@C@PANI

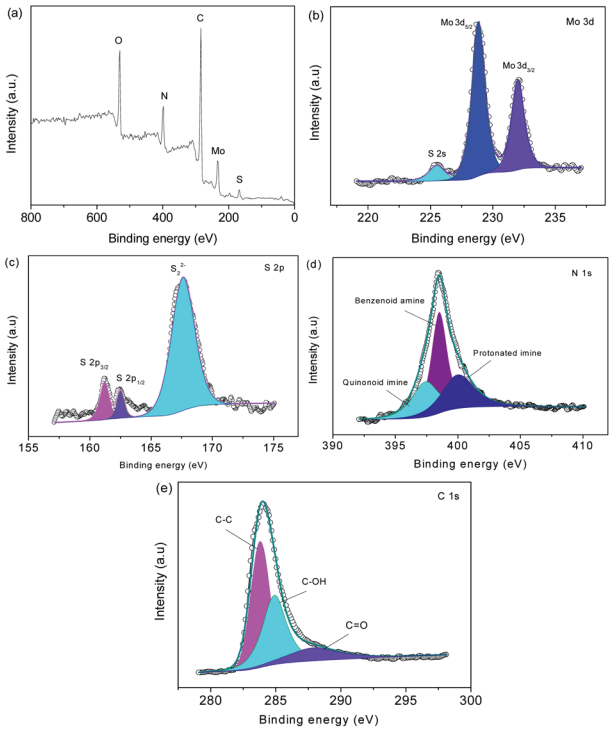

Fig. 6 (a) XPS survey spectrum, and (b) Mo 3d, (c) S 2p, (d) N 1s, and (e) C 2p spectra of MoS_2@C@PANI.

cathode. The anodic peaks around 0.6 to 1.2 and 1.9 V are ascribed to Mg^{2+} deintercalation, and the cathodic peaks at about 0.5, 1.25 and 1.75 V indicate the corresponding intercalation of Mg^{2+}.[27] The rate-performance at 0.1, 0.3, 0.5, and 1 A g^{-1} is displayed in Fig. 7d. It was repeatedly measured three times. The discharge capacity recovered to 143 mA h g^{-1} once the rate returned to 0.1 A g^{-1}. The battery after the high current density impact can maintain the capacity without obvious decrease. Fig. 8 shows the capacity at a low temperature of

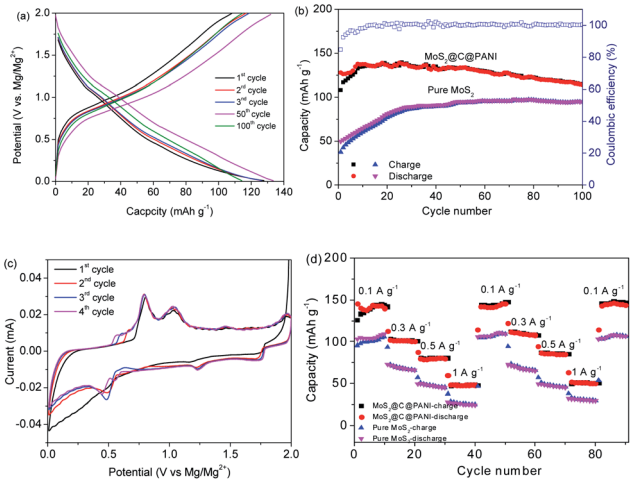

Fig. 7 (a) Charge–discharge curves of MoS_2@C@PANI at 0.1 A g^{-1}. (b) Capacities and coulombic efficiency. (c) CV curves cycled at 0.1 mA s^{-1}. (d) Rate-performance.

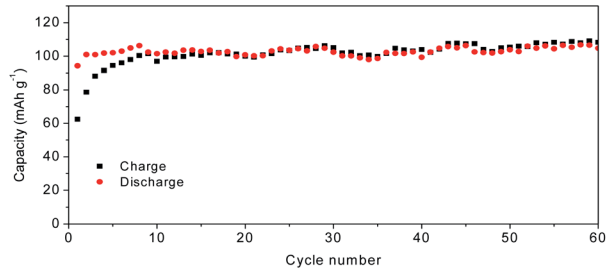

Fig. 8 Capacity of the MoS_2@C@PANI cathode cycled at 0.1 A g^{-1} at −5 °C.

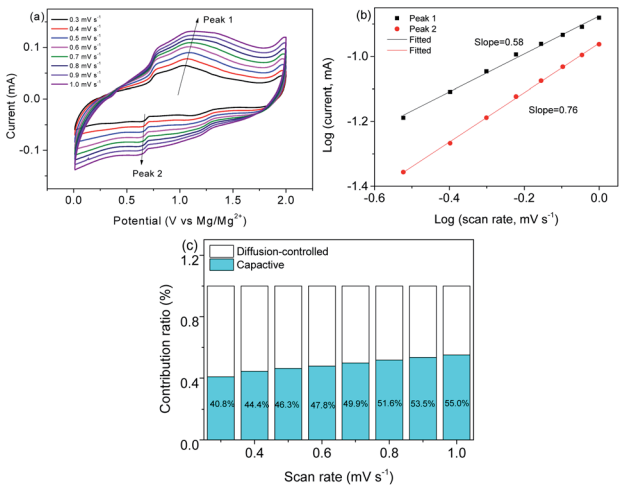

Fig. 9 (a) CV curves at different rates. (b) Log(v) to log(i) linear analysis. (c) Contribution ratios at different scan rates.

−5 °C. The initial Mg-storage capacity is relatively low, but it is stable. After cycling 60 times at 0.1 A g^{-1}, the capacity is 105 mA h g^{-1}. Furthermore, cycling at −10 °C (Fig. S1, ESI†) shows a capacity of about 98 mA h g^{-1}, indicating potential for use under cold conditions. The decreased capacity is ascribed to the reduced activity of electrode materials and the reaction kinetics of ions and electrolyte.[28–30]

Fig. 9a shows a series of CV curves which show that the peak position remains stable. Fig. 9b is obtained by fitting a qualitatively deduced charge storage equation $I(v) = av^b$,[26] where I stands for the maximum current.[31] The b of peak 1 and peak 2 is 0.58 and 0.76, respectively, indicating that charging and discharging are mainly controlled by the capacitance. On the basis of $i = k_1v + k_2v^{1/2}$, where k_1v/i and $k_2v^{1/2}/i$ are the capacitive and diffusion-controlled processes,[32] respectively, the contribution ratios are calculated (Fig. 9c). When the scan rates increase, the capacitive process increases. Fig. 10a and b show the SEM images of post-cycled MoS_2@C@PANI. This indicates that the composite remains robust after cycling 100 times. Fig. 10c shows the TEM image after 100 cycles, which further confirms that the structure remains stable after the charge–discharge cycles. The stability would be useful for constructing some dual-ion batteries. For example, a series of Ni/Zn–CoS_2@C and ternary metal oxide-based Mg–Li ion batteries displayed good stability.[33,34]

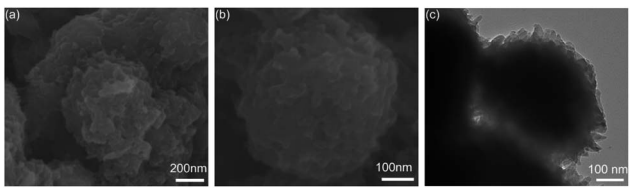

Fig. 10 (a and b) SEM and (c) TEM images of MoS_2@C@PANI after 100 cycles at 0.1 A g^{-1}.

Conclusions

In summary, we present a novel rose-with-thorn ternary MoS_2@C@PANI nanocomposite by coating carbon and PANI nanoneedles on rose-like MoS_2. The conductive PANI would enhance the conductivity of the system; MoS_2 is coated and protected by the coating, which enhances the electrochemical properties. The MoS_2@C@PANI-based Mg battery cathode shows a stable capacity of 114 mA h g^{-1} when cycled 100 times. Moreover, the cathode shows a recoverable rate-performance. At −5 °C, a capacity of 105 mA h g^{-1} is maintained, which indicates potential for use under cold conditions. It is expected that the biomimetic design and good performance presented here could be used for developing many other energy-storage materials and systems.

Conflicts of interest

There are no conflicts to declare.

Acknowledgements

This work was supported by the Science and Technology Major Project of Anhui Province (18030901093), Key Research and Development Program of Wuhu (2019YF07), Natural Science Research Project for Universities in Anhui Province (KJ2018ZD034, KJ2019A0502), Foundation of Anhui Laboratory of Molecule-Based Materials (FZJ21012), and the National Natural Science Foundation of China (21776121).

Notes and references

1 J. Yang, J. Wang, X. Dong, L. Zhu, D. Hou, W. Zeng and J. Wang, *Appl. Surf. Sci.*, 2021, **544**, 148775.
2 F. Bella, S. D. Luca, L. Fagiolari, D. Versaci, J. Amici, C. Francia and S. Bodoardo, *Nanomaterials*, 2021, **11**, 810.
3 M. Rashad, H. Z. Zhang, M. Asif, K. Feng, X. F. Li and H. M. Zhang, *ACS Appl. Mater. Interfaces*, 2018, **10**, 4757.
4 N. Narumoto, N. Okamoto and T. Saito, *J. Mater. Sci.*, 2021, **32**, 9990–9997.
5 R. Shah, V. Mittal, E. Matsil and A. Rosenkranz, *Adv. Mech. Eng.*, 2021, **13**, 16878140211003398.
6 W. Zhang, Y. Li, T. Lv, W. Liu, Y. Luo, R. Guo, H. Pei, C. Lai and J. Xie, *J. Electrochem. Soc.*, 2021, **168**, 030505.

7 X. Lin, J. Liu, H. Zhang, Y. Zhong, M. Zhu, T. Zhou, X. Qiao, H. Zhang, T. Han and J. Li, *Adv. Sci.*, 2021, **8**, 2002298.
8 C. Zuo, W. Tang, B. Lan, F. Xiong, H. Tang, S. Dong, W. Zhang, C. Tang, J. Li, Y. Ruan, S. Xi, Q. An and P. Luo, *Chem. Eng. J.*, 2021, **405**, 127005.
9 C. Du, W. Younas, Z. Wang, X. Yang, E. Meng, L. Wang, J. Huang, X. Ma, Y. Zhu and C. Cao, *J. Mater. Chem. A*, 2021, **9**, 3648–3656.
10 X. Xue, R. Chen, X. Song, A. Tao, W. Yan, W. Kong and Z. Jin, *Adv. Funct. Mater.*, 2021, **31**, 2009394.
11 K. Shen, Z. Zhang, S. Wang, Q. Ru, L. Zhao, L. Sun, X. Hou and F. Chen, *Energy Fuels*, 2020, **34**, 8987–8992.
12 X. Tao, J. Zhang, Y. Xia, H. Huang, J. Du, H. Xiao, W. Zhang and Y. Gan, *J. Mater. Chem. A*, 2014, **2**, 2290–2296.
13 C. Zuo, Y. Xiao, X. Pan, F. Xiong, W. Zhang, J. Long, S. Dong, Q. An and P. Luo, *ChemSusChem*, 2021, **14**, 2093–2099.
14 G. Y. Zhou, L. L. Mo, C. Y. Zhou, Y. Wu, F. L. Lai, Y. Lv, J. M. Ma, Y. E. Miao and T. X. Liu, *Chem. Eng. J.*, 2021, **420**, 127597.
15 C. X. Hou, W. Y. Yang, X. B. Xie, X. Q. Sun, J. Wang, N. Naik, D. Pan, X. M. Mai, Z. H. Guo, F. Dang and W. Du, *J. Colloid Interf. Sci.*, 2021, **596**, 396.
16 H. Sopha, A. T. Tesfaye, R. Zazpe, J. Michalicka, F. Dvorak, L. Hromadko, M. Krbal, J. Prikryl, T. Djenizian and J. M. Macak, *FlatChem*, 2019, **17**, 100130.
17 V. Panwar and S. L. Jain, *Mater. Sci. Eng. C*, 2019, **99**, 191–201.
18 S. Wang, F. Liu, C. Gao, T. Wan, L. Wang, L. Wang and L. Wang, *Chem. Eng. J.*, 2019, **370**, 322–329.
19 K. Zhang, Y. Xu, Y. Lu, Y. Zhu, Y. Qian, D. Wang, J. Zhou, N. Lin and Y. Qian, *J. Mater. Chem. A*, 2016, **4**, 6404–6410.
20 M. Ali, R. C. Guzman, O. Cojocari, S. Nellen, G. Santamaría, L. E. Garcia-Munoz, D. Segovia-Vargas, B. Globisch and G. Carpintero, *J. Infrared, Millimeter, Terahertz Waves*, 2019, **40**, 688–695.
21 C. Lv, S. Li, Y. Che, H. Chen, Y. Shu, J. He and J. Song, *Sep. Purif. Technol.*, 2021, **258**, 118048.
22 Y. Tian, M. Zhou, Y. Pan, X. Du and Q. Wang, *Chem. Eng. J.*, 2021, **403**, 126361.
23 Z. Wang, J. Zhang, T. Wen, X. Liu, Y. Wang, H. Yang, J. Sun, J. Feng, S. Dong and J. Sun, *Sci. Total Environ.*, 2020, **699**, 134341.
24 J. C. Wu, S. S. Chen, T. C. Yu, K. C. W. Wu and C. H. Hou, *Sep. Purif. Technol.*, 2021, **254**, 117561.
25 Z. Huang, L. Shi, Y. Muhammad and L. Li, *J. Colloid Interface Sci.*, 2021, **586**, 423–432.
26 C. L. Zuo, Y. Xiao, X. J. Pan, F. Y. Xiong, W. W. Zhang, J. C. Long, S. J. Dong, Q. Y. An and P. Luo, *ChemSusChem*, 2021, **14**, 2093.
27 L. Cui, L. Zhou, Y. M. Kang and Q. An, *ChemSusChem*, 2020, **13**, 1071–1092.
28 M. Asif, S. Kilian and M. Rashad, *Energy Storage Materials*, 2021, **42**, 129.
29 M. Rashad, H. Z. Zhang, X. F. Li and H. M. Zhang, *J. Mater. Chem. A*, 2019, **7**, 9968.
30 M. Rashad and M. Asif, *J. Energy Chem.*, 2021, **56**, 383.
31 X. Pu, T. Song, L. Tang, Y. Tao, T. Cao, Q. Xu, H. Liu, Y. Wang and Y. Xia, *J. Power Sources*, 2019, **437**, 226917.
32 A. Sihag, Z. L. Xie, H. V. Thang, C. L. Kuo, F. G. Tseng, M. S. Dyer and H. Y. T. Chen, *J. Phys. Chem. C*, 2019, **123**, 25618–25627.
33 M. Asif, M. Rashad and Z. Ali, *Nanoscale*, 2020, **12**, 14267.
34 M. Asif, M. Rashad, Z. Ali and I. Ahmed, *Nanoscale*, 2020, **12**, 924.